NANO LETTERS

2007
Vol. 7, No. 7
1973−1979

Hierarchical Placement and Associated Optoelectronic Impact of Carbon Nanotubes in Polymer-Fullerene Solar Cells

Sumit Chaudhary,[†,||] Haiwei Lu,[‡,||] Astrid M. Müller,[‡] Christopher J. Bardeen,[‡] and Mihrimah Ozkan*[,†]

Department of Electrical Engineering and Chemistry Department, University of California, Riverside, California 92521

Received March 27, 2007; Revised Manuscript Received May 22, 2007

ABSTRACT

Since their discovery, carbon nanotubes (CNTs) have been considered to be promising candidates for polymer-based solar cells, but their functional incorporation and utilization in such devices have been limited due to processing bottlenecks. Here, we demonstrate the realization of controlled placement of a single-walled CNT (SWNT) monolayer network at four different positions in polymer-fullerene bulk-heterojunction (BHJ) solar cells. SWNTs were deposited by dip-coating from a hydrophilic suspension, and a very brief, largely nondestructive argon plasma treatment of the active layer was utilized for incorporation of a SWNT layer within or above it. We demonstrate that SWNTs on the hole-collection side of the active layer lead to an increase in power conversion efficiency (PCE) of the photovoltaic devices from 4 to 4.9% (under AM 1.5 G, 1.3 suns illumination). This is the highest reported PCE for polymer-based solar cells incorporating CNTs, upon consideration of expected scaling of device parameters for 1 sun illumination. We also observe that SWNTs deposited on the top of the active layer lead to major electro-optical changes in the device functionality, including an increased fluorescence lifetime of poly-3-hexylthiophene (P3HT).

Organic photovoltaic (PV) cells offer promising technological advantages for actualization of low-cost and large-area fabrication on flexible substrates.[1] The state-of-the-art organic solar cells are based on the so-called donor−acceptor bulk-heterojunction (BHJ) devices that consist of a three-dimensional interpenetrating network of conjugated polymers and fullerene derivatives. To attain commercializable efficiencies, it is crucial that the solar energy is absorbed more efficiently in the active layer, requiring both a large thickness and a small energy gap of the active layers. However, short exciton diffusion lengths (∼10 nm) in these organic materials and challenges in achieving an optimized phase separation[2] for improved exciton-dissociation limit the thickness of the active-layer. Moreover, the fill-factor in these devices also suffers due to the short carrier drift length, $L_d = \mu\tau E$, where, μ is the carrier mobility, τ is the carrier recombination time, and E is the electric field. L_d must be longer than the active layer thickness to prevent significant losses by recombination. Approaches like post-production annealing[3] and slow-growth of spin-coated films[4] have been successfully utilized to tackle these issues.

An alternative approach in this direction is the introduction of one-dimensional (1D) nanostructures like carbon nanotubes (CNTs), which hold promise as exciton dissociating centers and ballistically conductive agents with high carrier mobilities,[5] in addition to being optically transparent, flexible, and environmentally resistant. However, their functional incorporation, characterization, and utilization in these devices have been limited[6−9] due to processing bottlenecks. The only reasonable success achieved has been with using a CNT layer as a replacement for the traditional transparent and hole-collecting electrode indium tin oxide (ITO), with 2.5% being the highest power conversion efficiency (PCE) reported until now.[10] Recently, PCEs exceeding 5% have been achieved in the polythiophene/methanofullerene based BHJ photovoltaic cells. In this wake, it has become increasingly intriguing to incorporate CNTs at different locations in these state-of-the-art-BHJ devices to characterize, reveal, and exploit their optoelectronic effects with regard to device performance and material properties.

In general, there are two ways to incorporate CNTs in a BHJ device configuration: layered assembly at desired locations or as a blend with the organic species. The success of the latter approach depends on appropriate chemical functionalization, individualization, and length-shortening of tubes, in addition to the optimization of their concentration

* Corresponding author. E-mail: mihri@ee.ucr.edu. Phone: (951) 827-2900.
[†] Department of Electrical Engineering.
[‡] Chemistry Department.
[||] These authors contributed equally to this work.

10.1021/nl070717l CCC: $37.00
Published on Web 06/15/2007

in organic composites. Associated chemical functionalization is normally via acid treatment, which tends to make these tubes hydrophilic and incompatible for blending with photoactive polymers,[11] besides creating many defects on the CNT side-walls and thus degrading their optoelectronic properties. Additive-assisted noncovalent approaches[12] can facilitate stable suspensions of CNTs, but they lack generality for optoelectronic purposes due to the presence of unwanted additives, e.g., surfactants. Realization of conductive CNT−network monolayers (spider-web approach[6]) from suspensions of pristine tubes is a relatively facile and promising approach to incorporate CNTs in sandwich-type organic devices. Filtering the solvent from CNT suspensions followed by lift-off of dried CNTs by poly(dimethylsiloxane) stamp and their subsequent transfer to substrate by printing has been shown to be a feasible methodology to realize these CNT networks.[6] However, this approach is not viable for printing CNTs on the top of polymeric species due to the inevitable mechanical degradation of such films by stamping.

Here we report a general and novel method of facilitating incorporation of SWNTs in P3HT/[6,6]-phenyl-C61-butyric acid methyl ester (PCBM) BHJ solar cells, and their characterization with regard to optoelectronic and photophysical effects. We fabricated several devices by precisely placing SWNTs at different hierarchical levels in the device structure, as shown in Figure 1a. Dip-coating from an additive-free suspension of mildly purified SWNTs in dimethylformamide (DMF) was utilized for this purpose. *ortho*-Dichlorobenzene (ODCB) and DMF have been shown to give the highest yields of individual pristine tubes in suspension formed by sonication and ultracentrifugation.[13] However, ODCB dissolves both P3HT and PCBM, which makes a ODCB−SWNT suspension incompatible for deposition on the P3HT/PCBM layer. Moreover, sonication of haloaromatic solvents such as ODCB also leads to the formation of sonopolymers,[13] which stay as undesired impurities in the suspension. Thus, we selected DMF suspension of SWNTs for our studies. Dip-coating from our DMF suspensions reproducibly yielded a monolayer of spider-web type SWNT network on glass or silicon substrates, as can be seen in Figure 1b. These monolayers consist of single tubes and their ropes, without any large bundles. The viability of this method is confirmed by the fact that deposition of these SWNT monolayers does not cause any short-circuiting of devices when another organic layer is spin-coated on them. Figure 1c shows that SWNTs in these DMF suspensions reveal more vibronic features than acid-oxidized tubes or surfactant-assisted aqueous suspensions of tubes, indicating the presence of a relatively high number of optoelectronically intact tubes and ropes in DMF. Note that modest-speed ultracentrifugation (16 000 rpm) was performed to remove large bundles, while concomitantly attaining a supernatant with reasonable concentration of individual tubes and ropes. High-speed ultracentrifugation process was avoided as it is reported to yield extremely low concentration of tubes in the supernatant (<20 mg/L),[12] which prevents high coverage of the substrate with the SWNT network using dip-coating deposition. Note that our

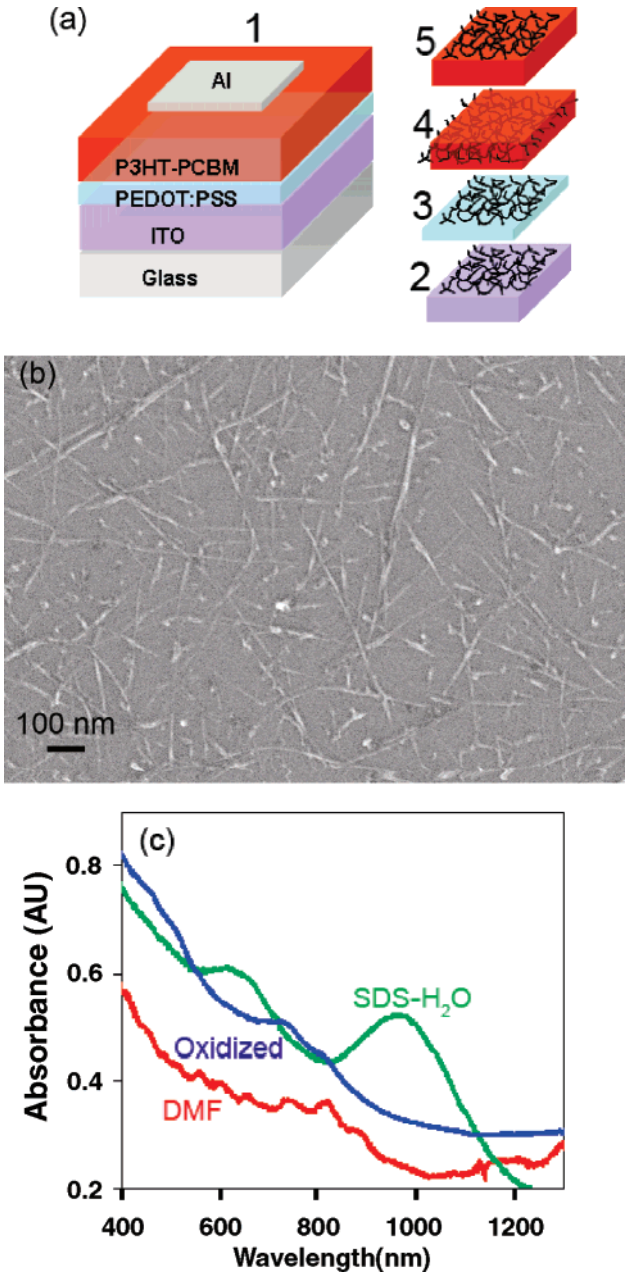

Figure 1. (a) Schematic of various devices fabricated in this work. No. 1 is the control device. Nos. 2−5 represent the layers from the respective devices on which the SWNT monolayer was dip-coated. For device 4, another active layer was spin-coated after the deposition of the SWNT layer on P3HT/PCBM, to effectively embed SWNTs in the P3HT/PCBM phase. (b) Monolayer of SWNT dip-coated on a Si substrate from a pristine DMF suspension. (c) UV−vis−NIR absorbance of SWNT suspension in DMF (red), SWNT−SDS suspension in water (blue), and acid-oxidized SWNTs in water (green).

DMF suspensions do not solely contain individual SWNTs, but they also contain ropes. Their presence, however, does not interfere with device stability. Therefore, these SWNT suspensions seem to offer great potential for PV devices.

Since DMF is a hydrophilic solvent, it shows good wettability and coverage on ITO and poly-3,4-ethylenedioxy-thiophene/polystyrene sulfonate (PEDOT/PSS) layers. Hence, device nos. 2 and 3 (Figure 1a) are realized without any further treatment of these layers prior to dip-coating.

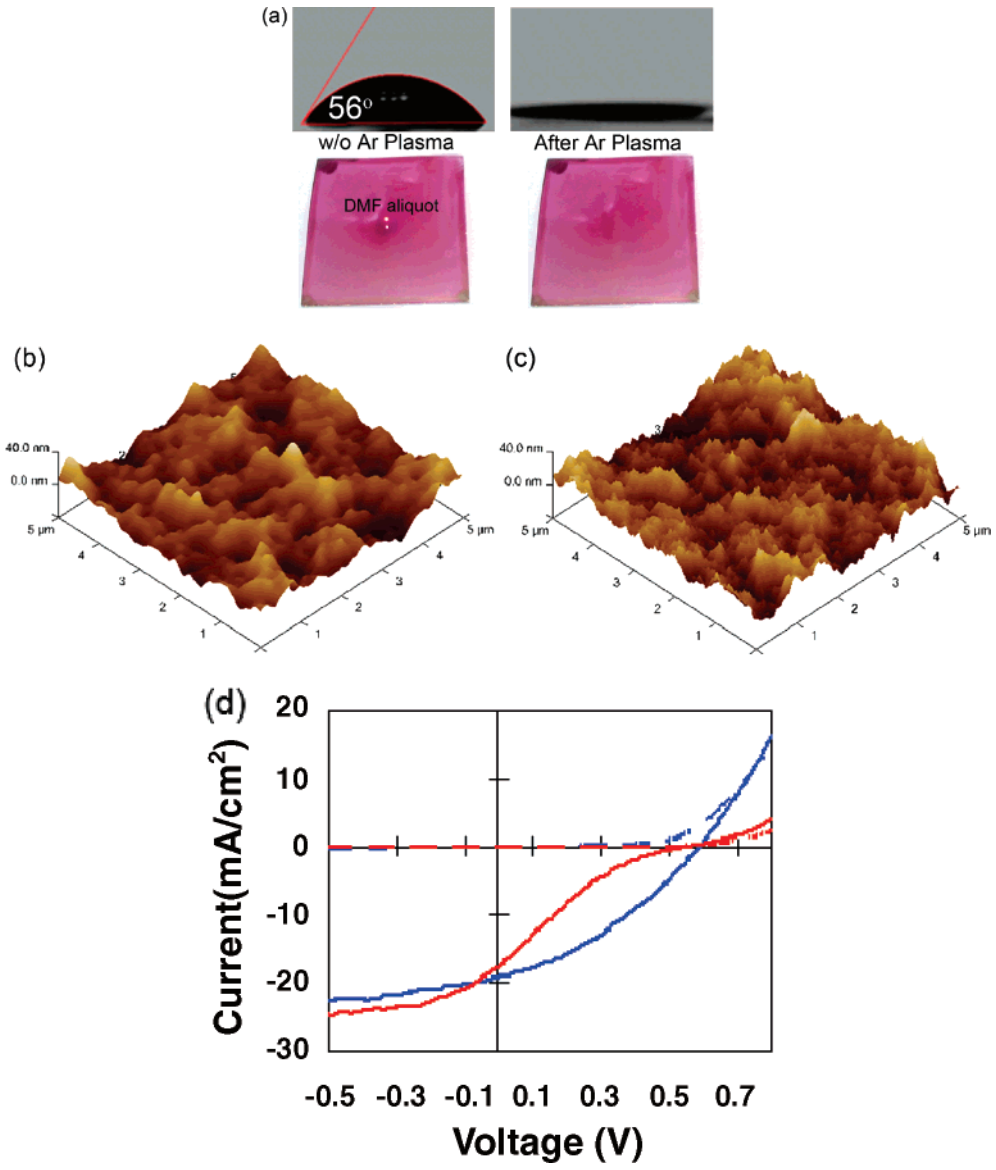

Figure 2. (a) Contact angle images and optical photographs of DMF aliquot on the P3HT/PCBM film without and with plasma treatment. (b) AFM height image of the P3HT/PCBM layer without plasma treatment, and (c) with mild Ar plasma treatment. Root-mean-square (rms) roughness was found to be similar for the control (9.3 ± 0.5 nm) and the layer treated with Ar plasma (9.0 ± 0.6 nm). (d) $I-V$ characteristics in dark (dotted lines) and under illumination (AM 1.5 G, 130 mW/cm^2) (solid lines) of the control device (no. 1) with (red) and without (blue) Ar plasma treatment of the active layer.

However, DMF shows poor wettability and high contact angle (~56°) on the hydrophobic P3HT/PCBM layer. To overcome this problem, we employed a novel approach. We exposed the active-layer to a very brief Ar plasma treatment (5 s exposure), which was dramatically able to change the wettability of DMF on the active layer, as shown in contact angle images in Figure 2a. Ar plasma was chosen over other gases because Ar is an inert gas, and Ar^+ ions do not form any network bonds with C or O atoms,[14] as oxygen or air plasma would be expected to do. In fact, much longer Ar plasma treatment (30 s exposure) of the PEDOT/PSS layer has even been shown to improve the fill-factor of organic-molecule solar cells.[15] Hence, we hypothesized that a 5 s exposure of Ar plasma will be largely nondestructive for the optoelectronic and structural properties of the active layer. The morphology of the active layer does not change after the brief Ar plasma as shown in Figure 2b. The film thickness, PL intensity, UV−vis absorbance intensity, and PL lifetimes of P3HT/PCBM also remain unaltered (results not shown). However, when the Al electrode is evaporated on the top of the plasma-treated active layer for the characterization of PV performance, a slight loss in photocurrent is observed, with I_{sc} and V_{oc} unaffected, as shown in the current−voltage ($I-V$) characteristics (Figure 2d). The reduction in photocurrent is attributed to the formation of minor charge traps induced by the plasma on the surface of the active layer, in the vicinity of exciton diffusion length from the Al electrode. However, since our objective is to tailor the surface energy for subsequent deposition of SWNTs, we expected that the reduction in photocurrent will not manifest itself after their deposition, and functionality introduced by SWNTs will be dominant. Moreover, post-

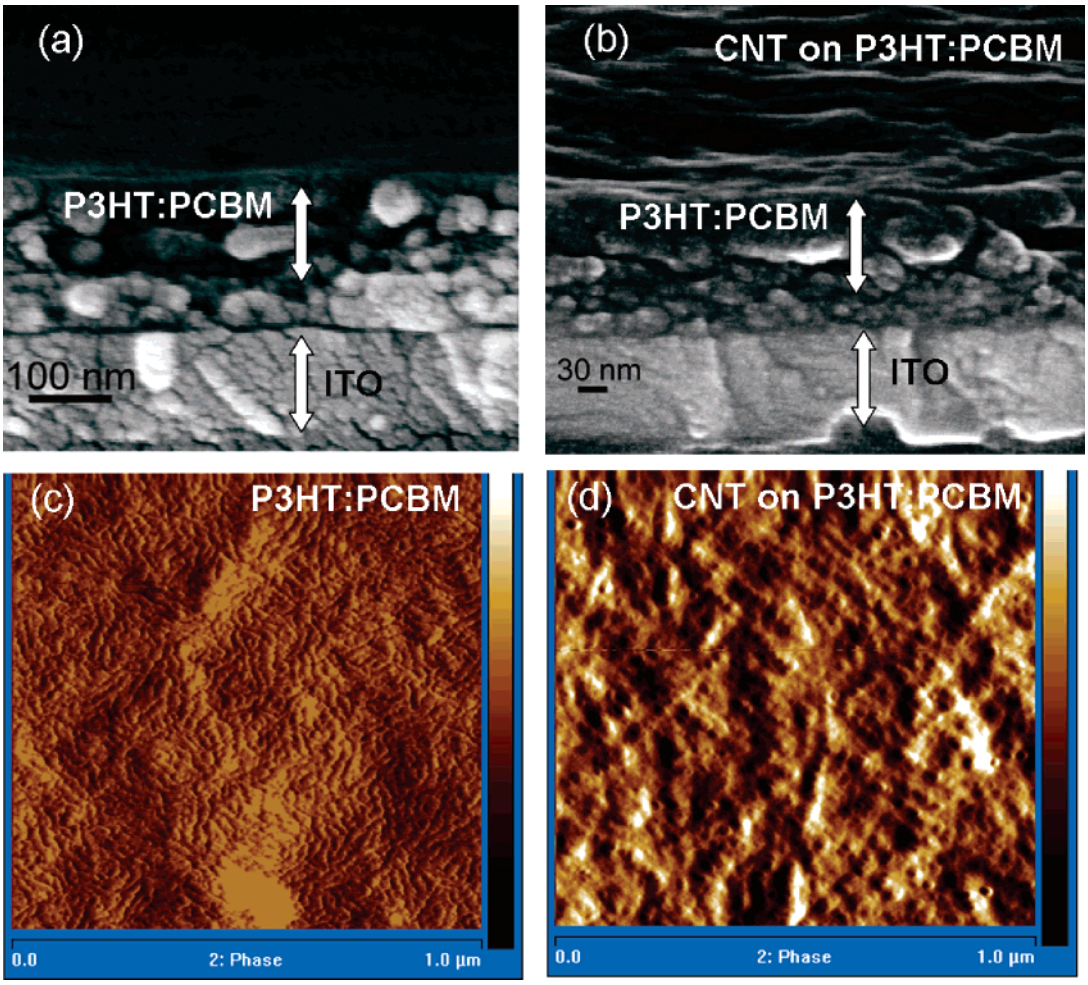

Figure 3. Left column: cross-sectional SEM (a) and AFM-phase image (c) of the P3HT/PCBM layer control device without SWNTs. Right column: corresponding images (b, d) of the configuration of device no. 5 with SWNT dip-coated on top of the P3HT/PCBM layer. rms roughness in both cases was found to be similar (P3HT/PCBM − 4.99 nm and CNT on P3HT/PCBM − 5.22 nm). Maximum scales in the AFM phase images are 50° (c) and 15° (d).

SWNT-deposition annealing can also remove the residual surface defects.

Figure 3 shows the cross-sectional scanning electron microscopy (SEM) and atomic force microscopy (AFM) phase images of the pristine P3HT/PCBM layer and the P3HT/PCBM layer with SWNTs dip-coated on top. It can be seen that SWNT deposition does not change the thickness or morphology of the active layer, although clear differences in the AFM phase images can be observed. For device no. 4, SWNTs are desired to be embedded effectively in the P3HT/PCBM layer. Hence, after a layer of SWNTs was deposited on the top of the active layer, another layer of P3HT/PCBM was spin-coated upon it. This step washes away the components of the bottom active layer through the porous SWNT network, and the overall film thickness of the active-layer remains unaltered (∼190 nm). Thus, in the aforementioned manner, we are successfully able to precisely place SWNT networks at different locations in the P3HT/PCBM BHJ PV devices.

The $I-V$ characteristics of our BHJ PV cells without and with SWNT layers are shown in Figure 4a, along with the summary of their performance parameters in Table 1. It can be seen that incorporation of SWNT layer on the cathodic side, either between ITO and PEDOT/PSS (device no. 2) or between PEDOT/PSS and the active layer (device no. 3) increases the PCE of these BHJ PV cells from 4% (control device without SWNTs) to 4.9% (under AM 1.5 G, 1.3 suns illumination). Increased fill factor (FF) and I_{sc} were responsible for the efficiency enhancement in device no. 2 and 3, respectively, in addition to increased V_{oc}. These improvements are also reflected in the values of series resistances (R_s) of the devices with device nos. 2 and 3 showing R_s values of 7.6 and 7.2 Ω cm^2, respectively, which are lower than the control device no. 1 (9.3 Ω cm^2). These SWNT-based devices show enhanced photocurrent as can bee seen in Figure 4b, which shows plots of photocurrent density vs voltage. These plots are effectively the difference between the $I-V$ characteristics under illumination and dark conditions. The improvements in I_{sc} or FF can be attributed to enhanced hole transport by the SWNTs network, which can provide conducting pathways to the electrode, while maximizing the surface area for collection of charges. Enhanced hole collection can also be partly ascribed to geometrical field enhancement at the SWNTs, which has been reported to be as great as 5-fold.[11] Increase in FF for device no. 2 also indicates a decrease in space−charge effects. Higher

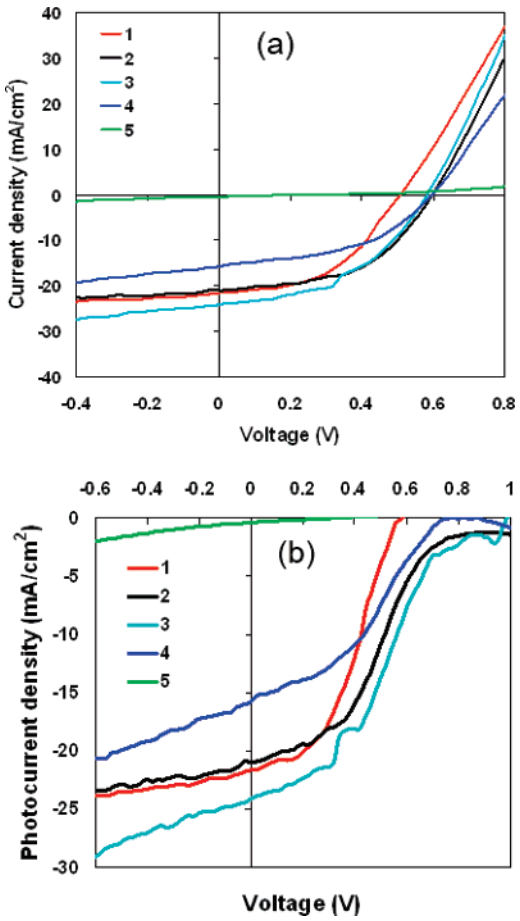

Figure 4. (a) $I-V$ characteristics of solar cells (device nos. 1−5) under AM 1.5 G illumination − 1.3 suns. (b) Photocurrent density vs voltage curves for the same devices. Photocurrent curves were obtained by subtracting the $I-V$ characteristics in the dark from $I-V$ characteristics under illumination.

Table 1. Summary of Device Characteristics for Various PV Devices Fabricated in This Work

device	V_{oc} (V)	I_{sc} (mA/cm^2)	FF	η(%)
1	0.51	21.6	0.47	4
2	0.59	21.0	0.51	4.9
3	0.59	24.1	0.44	4.9
4	0.59	15.7	0.47	3.3
5	0.27	0.40	0.25	0.01

V_{oc} for CNT-based devices can be attributed to reduced recombination losses[16] because the 1D nature of transport in CNTs is expected to reduce cul-de-sacs for holes.

It is known that I_{sc} increases linearly, but FF tends to reduce with increasing light intensity.[15] Hence, considering the scaling of I_{sc} and pessimistically assuming that no increase in FF will take place with reducing light intensity, our 4.9% efficient devices are still expected to show a PCE of ∼3.7% under 1 sun illumination.

Device no. 4 with SWNTs effectively embedded in the P3HT/PCBM shows a slight degradation in performance due to a reduction in I_{sc} (Figure 4a and Table 1). This is plausibly caused by decreased exciton dissociation in the active layer as SWNTs can disrupt the optimized[3,4] intimate contact between the P3HT and PCBM phases to some extent or act as quenching centers in the active layer. However, it should be noted that device no. 4 demonstrates the existence of photocurrent above the bias of 0.6 V, whereas control device (no. 1) does not, as shown in Figure 4b. Hence, incorporation of CNTs inside the BHJ active layer seems promising and requires further optimization. Device no. 5 with SWNT between the active layer and Al electrode shows drastic changes in device functionality with very low photocurrent. This is attributed to the work function of metallic SWNTs (∼5 eV), which is close to the work function of PEDOT/PSS (∼5.2 eV). This leads to a negligible electric field in device no. 5, and a flat-band condition already exists in short-circuit condition, rendering the device a nearly zero-field PV. This leads to a similar current in forward and reverse bias and an extremely low V_{oc} of 0.27 eV, as is expected from the difference in the work functions of metallic SWNTs and PEDOT/PSS. It should be noted that our SWNT layers consists of a mixture of semiconducting and metallic tubes. Generally, approximately one-third of tubes in a SWNT produce are metallic (work function $\varphi \sim 5$ eV), and few of them are expected to be in each rope, nominally 20 nm in diameter. Our results for device no. 5 suggest that consideration of metallic tubes seems enough to understand the changes in device parameters, with no obvious or discernible effect of band gaps of semiconducting tubes. It is not surprising as CNTs shift to a higher conductance level under electric field and semiconducting tubes can also approach semimetallic behavior.[17] One should note that, since minor variations in performance parameters are natural across devices within one set due to imperfect controllability, the performance parameters reported herein are representative of the best case of PCE across each set.

Optimized design of SWNT-based photovoltaics also calls for elucidation of photophysical impact of SWNTs, when in proximity with the polymer and methanofullerene species. Hence, we performed UV−vis absorption and time-resolved PL spectroscopy on the device structures utilizing the SWNT layer, embedded or adjacent to the active layer (Figure 5). UV−vis absorption spectra shows that the intensity and vibronic features of P3HT, including the longer wavelength feature (580−680 nm) ascribed to interplane stacking of P3HT chains,[18] remain unaltered for all device configurations where SWNTs are in intimate contact with the active layer. This suggests that incorporation of SWNT layers may not have as much optical impact on the polymeric phase. However, the shape and intensity of the absorption feature attributed to PCBM (280−380 nm) undergoes some shift in profile and intensity after the addition of the SWNT layer adjacent to or inside the active layer, as in the configuration of device nos. 3−5. This suggests that SWNTs may have some affinity to the fullerenes owing to a similar hexagonal carbon atom arrangement on their surface, and involved van der Waals forces.

To further reveal the photophysical effects of SWNTs, we probed the exciton dynamics of the active layer using PL lifetime measurements. The results are shown in Figure 5b, and the lifetime parameters are summarized in Table 2. It can be seen in Table 2 that blending of PCBM significantly

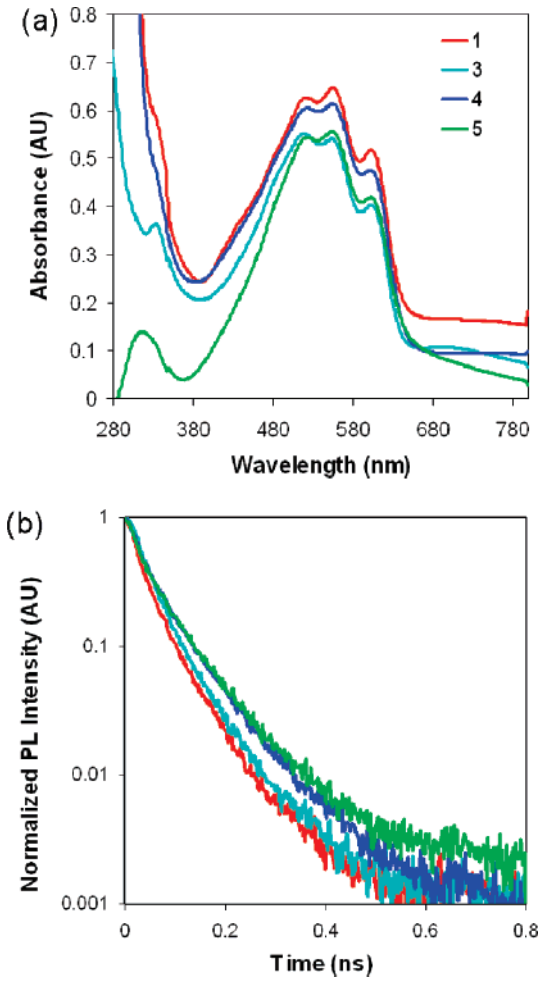

Figure 5. (a) UV−vis absorption spectra of active layers in the configuration of device nos. 1, 3, 4, and 5. (b) Fluorescence lifetime plots of the same set of devices. The legend of panel a also applies to panel b.

Table 2. PL Lifetimes (τ_1 and τ_2) and Integrated Intensities (A_1 and A_2) of the Two Decay Components for Several Films Investigated

film	pmT_1 (ps)	A_1	τ_2 (ps)	A_2
P3HT	91.1 ± 5.8	0.17	638.3 ± 3.1	0.83
P3HT/PCBM (1)	24.5 ± 0.4	0.57	70.5 ± 0.9	0.43
CNT below P3HT/PCBM (3)	32.5 ± 0.7	0.65	85.9 ± 2.1	0.35
CNT inside P3HT/PCBM (4)	29.8 ± 0.7	0.44	85.5 ± 0.9	0.56
CNT on P3HT/PCBM (5)	30.9 ± 0.8	0.51	94.7 ± 1.6	0.49

reduces the time constants of the biexponential PL decay of P3HT. The biexponential decay results from two distinct emitting species in the P3HT phase, most probably the longer chains in the film and photophysical aggregates.[19] However, introduction of SWNTs in the configurations of device nos. 3−5 slightly increases the PL lifetime, indicating that SWNTs affect the exciton dynamics. They lead to an increase in both time constants of P3HT PL decay, suggesting that SWNTs hinder the electron transfer from photoexcited P3HT to the PCBM phase. Preferential aggregation of PCBMs on SWNTs seems to be a plausible reason behind this. We believe that PL lifetime increases in the order of the SWNT configuration in device nos. 3−5 because of the increasing PCBM phase available for aggregation on SWNTs, as one goes up from the PEDOT/PSS layer to the Al electrode. This gradient in the PCBM phase is apparent from the SEM image in Figure 3a, where the particle size of the active layer is predominantly ∼15 nm (hydrodynamic radius of P3HT[20]) at the bottom, but larger aggregates ascribed to the PCBM phase can be seen near the top. The direct impact of our time-resolved PL studies cannot be clearly correlated to the device performance parameters, but the results can provide useful insights into the placement of SWNTs in the PV device structures.

In conclusion, we employed novel processing techniques to incorporate SWNT spider-web networks at various locations in the P3HT/PCBM BHJ PV devices and investigated their optoelectronic ramifications, including device performance and steady-state/dynamic photophysics. SWNTs on the cathodic side of the active layer lead to increased PCE with 4.9% being the highest value achieved, whereas SWNTs on the anodic side result into zero-field PV devices. Features of the PCBM phase in UV−vis absorption spectra are altered by the SWNTs and the time constants of biexponential PL decay are increased, showing that the femtosecond-scale exciton-dissociation process is affected when SWNTs are in intimate contact with the active layer. Our results are expected to be useful for the design of next generation CNT-based PV devices and for the improvement of processing conditions for further elucidation of their optoelectronic potential in organic devices.

Acknowledgment. S.C., H.L., and M.O. would like to thank the financial support of the Army, Riverside Public Utility and SCPPA.

Supporting Information Available: Experimental methods. This material is available free of charge via the Internet at http://pubs.acs.org.

References

(1) Shaheen, S. E.; Ginley, D. S.; Jabbour, G. E. *MRS Bull.* **2005**, *30*, 10.
(2) Kannan, B.; Castelino, K.; Majumdar, A. *Nano Lett.* **2003**, *3*, 1729−1733.
(3) Ma, W. L.; Yang, C. Y.; Gong, X.; Lee, K.; Heeger, A. J. *Adv. Funct. Mater.* **2005**, *15*, 1617−1622.
(4) Li, G.; Shrotriya, V.; Huang, J.; Yao, Y.; Moriarty, T.; Emery, K.; Yang, Y. *Nat. Mater.* **2005**, *4*, 864−868.
(5) Pradhan, B.; Batabyal, S. K.; Pal, A. J. *Appl. Phys. Lett.* **2006**, *88*, 093106−093108.
(6) Gruner, G. *J. Mater. Chem.* **2006**, *16*, 3533−3539.
(7) Lagemaat, J.; Barnes, T.; Rumbles, G.; Shaheen, S. E.; Coutts, T. J.; Weeks, C.; Levitsky Peltola, J.; Glatkowski, P. *Appl. Phys. Lett.* **2006**, *88*, 233503−233505.
(8) Pasquier, A. D.; Unalan, H. E.; Kanwal, A.; Miller, S.; Chhowalla, M. *Appl. Phys. Lett.* **2005**, *87*, 203511−203513.
(9) Kymakis, E.; Alexandrou, I.; Amaratunga, G. A. J. *J. Appl. Phys.* **2003**, *93*, 1764−1768.
(10) Rowell, M. W.; Topinka, M. A.; McGehee, M. D.; Prall, H.; Dennler, G.; Sariciftci, N. S.; Hu, L.; Gruner, G. *Appl. Phys. Lett.* **2006**, *88*, 233506−233508.
(11) Miller, A. J.; Hatton, R. A.; Silva, S. R. P. *Appl. Phys. Lett.* **2006**, *89*, 133117−133119.
(12) O'Connell, M. J.; Bachilo, S. M.; Huffman, C. B.; Moore, V. C.; Strano, M. S.; Haroz, E. H.; Rialon, K. L.; Boul, P. J.; Noon, W. H.; Kittrell, C.; Ma, J.; Hauge, R. H.; Weisman, R. B.; Smalley, R. E. *Science* **2002**, *297*, 593−597.

(13) Kim, D. S.; Nepal, D.; Geckeler, K. E. *Small* **2005**, *1*, 1117−1124.
(14) Tay, B. K.; Sheeja, D.; Lau, S. P.; Guo, J. X. *Diamond Relat. Mat.* **2003**, *12*, 2072.
(15) Peumans, P.; Forrest, S. R. *Appl. Phys. Lett.* **2001**, *79*, 126−128.
(16) Wienk, M. M.; Kroon, J. M.; Verhees, W. J. H.; Knol, J.; Hummelen, J. C.; van Hal, P. A.; Janssen, R. A. J. *Angew. Chem., Int. Ed.* **2003**, *42*, 3371.
(17) Chen, C.; Lee, M.; Clark, S. J. *Nanotechnology* **2004**, *15*, 1837.
(18) Kim, Y.; Cook, S.; Tuladhar, S. M.; Choulis, S. A.; Nelson, J.; Durrant, J. R.; Bradley, D. D. C.; Giles, M.; McCulloch, I.; Ha, C.; Ree, M. *Nat. Mater.* **2006**, *5*, 197−203.
(19) Schwartz, B. J. *Annu. Rev. Phys. Chem.* **2003**, *54*, 141−72.
(20) Hoppe, H.; Sariciftci, N. S. *J. Mater. Chem.* **2006**, *16*, 45−61.

NL070717L